coatings

MDPI

Article

A Mechanism of Anti-Oxidation Coating Design Based on Inhibition Effect of Interface Layer on Ions Diffusion within Oxide Scale

Bo Yu [1,2], Ya Liu [3], Lianqi Wei [1,4], Xiaomeng Zhang [1,4], Yingchao Du [1,2], Yanhua Wang [1,2] and Shufeng Ye [1,4,*]

1 State Key Laboratory of Multiphase Complex System, Institute of Process Engineering, Chinese Academy of Sciences, PO Box 353, Beijing 100190, China; yubo@ipe.ac.cn (B.Y.); lqwei@ipe.ac.cn (L.W.); xmzhang@ipe.ac.cn (X.Z.); ycdu@ipe.ac.cn (Y.D.); wangyhhg@163.com (Y.W.)
2 Department of Chemical Engineering, University of Chinese Academy of Sciences, No. 19(A) Yuquan Road, Beijing 100049, China
3 Dalian Research Institute of Petroleum and Petrochemicals, Sinopec Corporation, No. 96 Nankai Road, Dalian 116045, China; 13141240623@163.com
4 Innovation Academy for Green Manufacture, Chinese Academy of Sciences, Beijing 100190, China
* Correspondence: sfye@ipe.ac.cn; Tel.: +86-1391182846

Abstract: In this paper, a mechanism of anti-oxidation coating design based on the inhibition effect of the interface layer on the diffusion of ions within oxide scale was introduced. The Fe^{2+} ions diffusion behavior in Fe_3O_4, Cr_2FeO_4, and $FeAl_2O_4$ were studied by molecular dynamics method of Nudged elastic bond. As the result shown, Fe^{2+} ions tended to diffuse through the vacancy at tetrahedral site in Cr_2FeO_4 and $FeAl_2O_4$, but diffuse through the octahedral vacancy in Fe_3O_4. When temperature ranged from 1073 to 1325 K, the energy barrier of Fe^{2+} ions diffusion in Cr_2FeO_4 was higher than that of $FeAl_2O_4$, and both of that were still obvious higher than that in Fe_3O_4. A new anti-oxidation coating was prepared based on the inhibition of interface layer consisted of $FeAl_2O_4$ to protect the carbon steel S235JR at 1200 °C for 2 h. The $FeAl_2O_4$ region was formed and observed at the interface between coating and Fe element diffusion area, and the mullite phase was distributed outside of the $FeAl_2O_4$ region. Comparing to the bare sample, the prepared coating exhibited an excellent anti-oxidation effect.

Keywords: anti-oxidation coating; metal oxidation; ions diffusion; carbon steel

Citation: Yu, B.; Liu, Y.; Wei, L.; Zhang, X.; Du, Y.; Wang, Y.; Ye, S. A Mechanism of Anti-Oxidation Coating Design Based on Inhibition Effect of Interface Layer on Ions Diffusion within Oxide Scale. *Coatings* **2021**, *11*, 454. https://doi.org/10.3390/coatings11040454

Academic Editor: Daniel de la Fuente

Received: 28 February 2021
Accepted: 11 April 2021
Published: 14 April 2021

1. Introduction

In order to reduce the damage caused by the serious oxidation during the reheating process before hot rolling, temporary protective coating is usually utilized due to its low price and easy operation [1–3]. Recently, most of the research are depended on the preparation and the anti-oxidation of the coating [4,5], but there are few reports about the ideas of the anti-oxidation coating design. Referring to the theory of metal oxidation at high temperature, a mechanism of anti-oxidation coating design based on the inhibition effect of the interface layer on the diffusion of ions within oxide scale was introduced in this paper. According to the mechanism, a new ceramic coating was prepared to protect the carbons steel S235JR at 1200 °C for 2 h. The mechanism was verified with the anti-oxidation effect of the coating and structure of the interface layer.

The oxidation law of metal at high temperature was the basis of the anti-oxidation design. As we all known, there were two main stage during the oxidation of the metal at high temperature. At the initial stage, the oxidation rate was controlled by the reaction resulted from the direct contact between the oxygen and substrate and the kinetics could be expressed by linear law [6]. As the reaction went on, the oxide scale gradually turned thicker, and the kinetics followed the parabolic law, which meant that the ions diffusion played a significant role at this stage [6]. However, the current anti-oxidation coatings

were designed mainly based on the isolation effect of the coating on the oxygen diffusion. Liu studied the oxidation behaviour of 304 stainless steel [7]. The result showed that the oxide scale formed on the surface of 304 stainless steel consisted of Cr_2FeO_4, which could effectively inhibit the ions diffusion during oxidation at high temperature. Therefore, the oxidation rate of 304 stainless steel was mainly controlled by the oxidation process. According to the result above, Liu et al. prepared a kind of glass-based anti-oxidation coating [7], which could form a molten film on the surface of 304 stainless steel, isolating the direct contact between oxygen and the substrate, thus achieving an excellent protective effect. In this paper, we mainly focused on designing the coating to protect the carbon steel S235JR with the oxide scale consisted of FeO and Fe_3O_4 from oxidation. Because the oxide scale lacked the inhibition effect of Cr_2FeO_4 on ions diffusion, the coating designed based on the isolation effect of the coating on the oxygen diffusion was not applicable. In a study operated by Abluwefa et al., it was found that the oxygen level significantly affected the initial oxidation rate, but had no effect on the subsequent parabolic oxidation rate [8]. Therefore, it was the diffusion of ions rather than the oxygen affected the oxidation rate at high temperature.

In addition to environment factors such as temperature and holding time, ions diffusion was mainly affected by the structure of the scale. Most important of all, the type of defects in the scale structure could be used to determine which ions dominate the diffusion process. Chen et al. reviewed the oxidation law and scale structure formed of pure iron and carbon steel at high temperature. According to this revision, within the parabolic regime, the scale of pure iron at high temperature was composed of FeO, Fe_3O_4, and Fe_2O_3. The scale structure of carbon steel was similar to that of pure iron [9–12], but the relative proportion of FeO layer and Fe_3O_4 layer was different due to the blisters caused by the CO and CO_2 generated from the oxidation of element C [12,13].

Both the FeO and Fe_3O_4 were p-type semiconductors, in which the defects were mainly the vacancies of cationic. Therefore, the diffused ions were mainly Fe^{2+} and Fe^{3+} ions [14]. Referring to the principle of crystal field, the crystal field stability energy of Fe^{2+} ions is significantly higher than that of Fe^{3+}. When cations vacancy occurred in the scale, Fe^{2+} ions would be prone to diffuse. Same conclusion could result from the research carried out by Frolich and Stiller. According to the research, hybridized bond form at tetrahedral site could be expressed as $4s^1 3d^3[t_{2g}]^4[e_g]$, there possibly were orbital overlap as well as lone pair electrons. However, the hybridized bond form at octahedral site could be expressed as $4s^1 3d^2[e_g]^2[t_{2g}]4p^3$, neither the orbital overlap nor lone pair electrons were under this condition. As a result, Fe–O bond at tetrahedral site tended to be covalent, but that at octahedral tended to be ionic [15]. It could be inferred that cationic vacancies were prone to form at octahedral site due to the breaking of Fe–O bond at octahedral site.

Except for pure iron and carbon steel, the oxidation law of 304 stainless steel was also closely related to its scale structure. The scale structure of 304 stainless steel was mainly consisted of Cr_2FeO_4. It was widely known that the oxidation resistance of 304 stainless at high temperature was result from the Cr_2FeO_4 layer [7,16], but there were few report made clear whether the isolation from the oxygen or the inhibition effect on the ions diffusion gave rise to the anti-oxidation effect. In his research, Dickman focused on the diffusion law of Fe^{2+} ions in Fe_3O_4 and Cr_2FeO_4 by isotope tracer method of Fe^{59}. As the result showed, the diffusion rate of Fe^{2+} ions in Cr_2FeO_4 was much lower than that of Fe_3O_4. According to the result above, it could be inferred that the anti-oxidation property of 304 stainless steel mainly resulted from the inhibition effect of Cr_2FeO_4 on the diffusion of Fe^{2+} at high temperature.

According to the correlation between the scale structure and oxidation property of the metal at high temperature, the oxidation could be protected if in situ reaction could be built to generate an interface layer instead of the scale consisted of FeO and Fe_3O_4. Referring to the crystal structure of Cr_2FeO_4, it seemed easy to search a suitable crystal structure of interface layer. Cr_2FeO_4 and Fe_3O_4 were both the spinel with space group $Fd\bar{3}m$; however, the distribution of Fe^{2+} ions were different. In the crystal lattice of Cr_2FeO_4,

Cr^{3+} ions occupied the octahedral site, while Fe^{2+} ions filled the tetrahedral space. In the crystal lattice of Fe_3O_4, half of the Fe^{3+} ions and all the Fe^{2+} ions occupied the octahedral site, while the other Fe^{3+} ions filled the tetrahedral space. According to the report of Frolich and Stiller [15], Fe–O bond in octahedral site in the crystal lattice of Fe_3O_4 were prone to break and generated cation vacancy. In addition, the Fe^{2+} ions were prone to diffuse through the cation vacancy at octahedral site based on the research of Dickman [14]. Therefore, it was possibly to infer that a crystal lattice with less Fe^{2+} ions at octahedral site contributed to inhibition effect on Fe^{2+} ions diffusion, such as $FeAl_2O_4$ which could be expressed as $(Fe^{2+}_{0.77}Al^{3+}_{0.23})_{tet}(Fe^{3+}_{0.07}Fe^{2+}_{0.05}Al^{3+}_{0.88})_{2oct}O_4$ according to the research operated by Jastrzebska [17]. Odashima et al. prepared a kind of anti-oxidation coating for 3% Si-steel [18]. In his work, $FeAl_2O_4$ was firstly introduced as functional components to improve the anti-oxidation effect, but the mechanism of inhibition effect of $FeAl_2O_4$ was not further studied.

With the development of computation science, the study of ions diffusion behavior could be researched by molecular dynamics. In this paper, the Fe^{2+} ions diffusion behavior in Fe_3O_4, Cr_2FeO_4, and $FeAl_2O_4$ were studied by molecular dynamics method of Nudged elastic bond. The diffusion path of Fe^{2+} ions were analyzed by comparing the cationic defect formation energy at tetrahedral and octahedral sites in the crystal lattice above. The Fe^{2+} ions diffusion energy barrier under the corresponding path conditions were calculated to verify the inhibition effect of Cr_2FeO_4 and $FeAl_2O_4$ on Fe^{2+} ions diffusion at high temperature. A new anti-oxidation coating was prepared based on the inhibition of interface layer consisted of $FeAl_2O_4$ to protected the carbon steel S235JR at 1200 °C for 2 h. The protective effect of the coating was investigated, and the mechanism based on the inhibition effect of interface layer was verified by the distribution of elements in the coating cross-section and the structure of interface layer.

S235JR was a kind of most common carbon steel, the reheating temperature before hot rolling usually ranged from 1100 to 1250 °C based on the size of the billet, which was closed to that of most other kinds of carbon steel. There was only trace element of Si and Mn, which had no obvious influence on the structure of the scale. S235JR was selected as the protected object in this paper, which could ensure the universality of the obtained mechanism suitable for most kind of carbon steel and low alloy steels with the scale consisted of FeO, Fe_3O_4, and Fe_2O_3. If some other kinds of steel, of which the kinetics followed by parabolic law, was selected as protective object, anti-oxidation coating could be designed and prepared by the method obtained in this paper. Therefore, this paper mainly provided method of anti-oxidation design based on the inhibition effect of interface layer on ions diffusion at high temperature, which had significance of guidance and reference.

2. Materials and Methods

2.1. Methodology of the Molecular Dynamics

In order to calculate the diffusion paths and energy barriers of an Fe^{2+} ion in Fe_3O_4, Cr_2FeO_4 as well as in $FeAl_2O_4$ crystals, three 2a × 2a × 2a (a is the lattice constant for Fe_3O_4, Cr_2FeO_4 or $FeAl_2O_4$) supercells are created for these three crystals with space group $Fd\bar{3}$-m [17]. A substitutional vacancy is introduced to the crystal by randomly deleting one of the Fe^{2+} ions at the octahedral site or tetrahedral site. The crystal structure before and after the vacancies formation was shown as Figure 1.

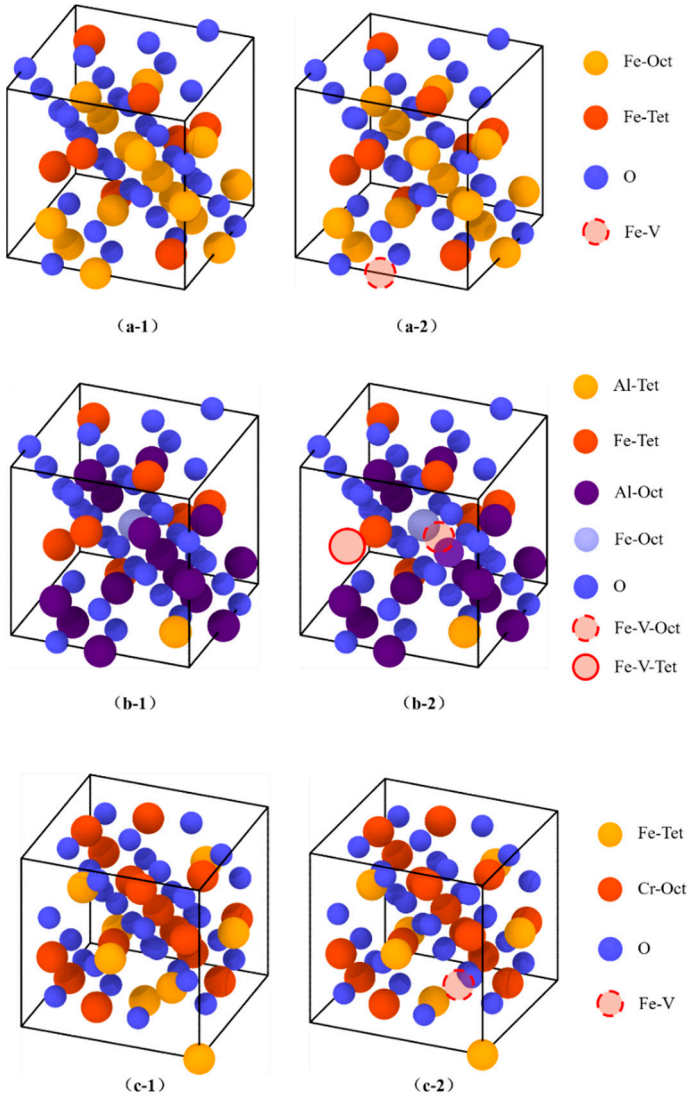

Figure 1. Schematic of crystal structure (**a-1**) Fe_3O_4 without any vacancy (**a-2**) Fe_3O_4 with octahedral vacancy (**b-1**) $FeAl_2O_4$ without any vacancy (**b-2**) $FeAl_2O_4$ with tetrahedral or octahedral vacancy (**c-1**) Cr_2FeO_4 without any vacancy (**c-2**) Cr_2FeO_4 with tetrahedral vacancy.

The path and energy transition of an Fe^{2+} ion diffusing towards the vacancy at 0 K are determined by the nudged elastic band (NEB) method [19]. Five atomic locations are identified, including the starting/ending octahedral sites and 3 transitional sites along the diffusion path for Fe_3O_4 and $FeAl_2O_4$, the starting/ending tetrahedral sites and 3 transitional sites along the diffusion path for Cr_2FeO_4 and $FeAl_2O_4$. After determination of the diffusion path, the energy barriers of the diffusing Fe^{2+} ion under finite temperatures are calculated. Five simulations are conducted at each temperature (i.e., 1073 K, 1173 K, 1273 K, 1373 K, 1473 K, and 1523 K), corresponding to the Fe^{2+} ion initially located at the 5 sites along its diffusion path. The systems are allowed to equilibrate at the given temperature. In this case, the Fe^{2+} ion will gradually diffuse to its stable locations under the thermodynamic driving force. The evolution of system energy is monitored and the corresponding energy barrier under the specific temperature can thus be calculated.

In these study, the charge transfer ionic potential (CTIP) originally proposed by Zhou et al. is adopted as the interatomic force filed [20]. Such a force filed has received wide applications and proved to be accurate in handling both ionic and covalent materials [21,22]. In this potential, the system energy consists of two parts of contributions, i.e., the electrostatic part and the non-electrostatic part. A charge equilibration (Qeq) procedure

is applied during the simulation to accurately capture the ionic interactions. A 12Å cutoff radius is adopted, and the Qeq minimization is performed at each time step. Throughout this study, a Nosé–Hoover thermostat is used and a 1 fs simulation time step is chosen. All simulations are performed using the open source software LAMMPS (V.2014) [22] and structures are visualized using Ovito (V.2.9.0) software [23].

2.2. Experimental Details

2.2.1. Preparation of the Sample

Carbon steel, S235JR, with a specimen size of 10 × 10 × 10 mm^3 was used for evaluating the oxidation resistance performance of anti-oxidation coating. The composition of S235JR was listed in Table 1. The samples were polished by abrading with SiC papers from 200# grit to 1200# grit, and then cleaned through an ultrasonic treatment.

Table 1. Chemical composition of carbon steel S235JR.

Element	C	Si	Mn	S	P	Fe
Wt.%	0.20	0.35	1.40	≤0.045	≤0.045	balance

2.2.2. Preparation of the Coating Slurry

Different with general ceramic powders, $FeAl_2O_4$ existed in nature however was rarely found; thus, $FeAl_2O_4$ could only be obtained by artificial synthesis [24–26]. The reaction between Al_2O_3 and Fe_3O_4 could generate $FeAl_2O_4$, which is the simplest way to obtain the $FeAl_2O_4$ (Equations (1) and (2)). However, this reaction is difficult to occur at low temperature and usually needs to be heated to more than 1400 °C or directly depends on electric fusion.

$$Al_2O_3 + Fe_3O_4 \rightarrow FeAl_2O_4 + Fe_2O_3 \quad (1)$$

$$2Al_2O_3 + Fe_3O_4 \rightarrow FeAl_2O_4 + Fe_2O_3{\cdot}Al_2O_3(ss) \quad (2)$$

According to the above reactions, the $FeAl_2O_4$ can also be synthesized through the reaction between Fe_3O_4 and raw mineral materials containing Al_2O_3. In the process of using aluminum-based refractories, $FeAl_2O_4$ usually exists as transition phase at the interface between the refractory brick and the metal oxide layer or molten metal iron. Therefore, mullite containing Al_2O_3 are selected as principle raw materials of coating slurry in this paper. Sodium silicate was selected as binder in this paper. On one hand, dehydration and condensation of silanols could form inorganic polymer network, which could increase the curing property of coatings at room temperature. On the other hand, the amorphous SiO_2 exhibited excellent reactivity, which could improve the sintering of the ceramic particles [27]. Sodium polyacrylate was used as dispersant in this paper. In the dispersed system of ceramic clay and water, there was a large number of diffuse double electric layers on the surface of the ceramic clay. There were a lot of carboxyl groups on the main chain of sodium polyacrylate. When sodium polyacrylate solution severed as dispersant, the ceramic particles would be suspended and dispersed due to the charge repulsion [28]. The ceramic coating was prepared to prevent the carbon steel S235JR from oxidation at 1200 °C for 2 h. The composition of ceramic coating slurry is shown in Table 2.

Table 2. Composition of ceramic coating slurry.

Components	Mullite Powders	Sodium Silicate Solution	Sodium Polyacrylate	Water	Components
Wt.%	0.20	0.35	1.40	≤0.045	≤0.045

The above raw materials were added to a beaker in the proportion as shown in Table 1 and mixed under magnetic stirring at 500 $r{\cdot}min^{-1}$ for 30 min. The prepared coating slurry

was sprayed onto the surface of S235JR sample. The sample size was 10 mm × 10 mm × 10 mm, and the thickness of coating was about 0.4 mm.

2.2.3. Evaluation of the Anti-Oxidation Coating

The bare and coated samples of S235JR were placed into a continuous thermos-balance (RZ, Luoyang Precondar, Luoyang, China), respectively. The samples were heated from room temperature to 1200 °C at a rate of 10 °C·min^{-1} and maintained for 2 h. The counting interval was set for 1 min, and the oxidation weight gain of the samples during heating process was recorded continuously.

The oxidation kinetics of the substrate usually followed the linear law at the initial stage of oxidation, namely, the oxidation rate was controlled by the oxidation reaction, which was relative to the partial pressure of oxygen. In this case, the oxidation kinetic equation should follow the linear rule, and its expression was shown in Equation (3). Here, the Δω was the weight gain of sample per unit area (mg·cm^{-2}), H was a constant, k_t was the oxidation reaction rate constant (mg·cm^{-2}·s^{-2}), ti was the reaction time (min). A linear fitting curve of Δω versus t_i could be plotted, and the slope of the curve is the oxidation reaction rate constant of k_s.

$$\Delta\omega = H + k_t \times t_i \quad (3)$$

When the oxide layer reached to a certain thickness, the reaction rate was controlled by the diffusion of Fe^{2+} ions. In this case, the oxidation kinetic equation should follow the parabolic rule, and its expression was shown in Equation (4). Here, the Δω was the weight gain of sample per unit area (mg·cm^{-2}), H was a constant, k_p was the oxidation reaction rate constant at stage for parabolic law (mg^2·cm^{-4}·s^{-2}), t_i was the reaction time (min). A linear fitting curve of $(\Delta\omega)^2$ versus t_i could be plotted, and the slope of the curve is the oxidation reaction rate constant of k_p.

$$(\Delta\omega)^2 = H + k_p \times t_i \quad (4)$$

The weight gain data during the temperature-holding stage at 1200 °C could be fitted by the method as follow. Frist of all, we set a time node per 5 min from 5 to 115 min, because at least 5 points were needed to ensure the accuracy of the curve fitting. The weight gain data from 0 min to the time node was fitted by the linear law, while that from time node to 120 min was fitted by the parabolic law. Both of the correlation coefficients were recorded when the time node changed from 5 to 115 min. By comparing the correlation coefficient, the time node was determined, and the oxidation weight gain data was fitted by different stages with linear law and parabolic law.

The anti-oxidation effect of the coating could be intuitively observed through the oxidation weight gain curve of the bare and coated sample. The inhibition effect of the prepared coating on the diffusion of Fe^{2+} ions at high temperature could be evaluated by comparing the oxidation reaction rate constant of the bare and coated sample in the temperature-holding stage.

X-ray diffractometer was engaged to determine the phase formed on the inner-face of the coating, proving the formation of the $FeAl_2O_4$ interface layer. The element distribution at cross section of the bare and coated sample was characterized by Scanning electron microscopy equipped with an Energy Dispersive X-ray Spectroscopy to analyze the composition of the interface layer between the coating and carbon steel substrate and verify whether the designed reaction path of $FeAl_2O_4$ was rational or not. According to the difference of Fe distribution, the inhibition effect of interfacial layer structure on the diffusion of Fe^{2+} ions at high temperature could be further investigated.

The experimental instruments used in this study were listed in Table 3.

Table 3. Experimental instruments.

Instruments	Model	Manufacturer
Electronic balance	ME204/02	Mettler Toledo (Tokyo, Japan)
Heat collection type magnetic stirrer	DF-101S	Gongyi Yu Hua Instrument Co., Ltd (Gongyi, China)
Thermal field emission scanning electron microscope	JSM-7001F	Japan Electrics Co.,Ltd (Tokyo, Japan)
Energy spectrum analyzer	INCA X-MAX	Oxford (Tokyo, Japan)
Ultrasonator	PS3200	Shaanxi Puluodi (Xian, China)
Muffle furnace	BFX-16A	FLAME (Tokyo, Japan)
X-ray diffractometer	X'Pert PRO MPD	PANalytical B. V. (Almelo, The Netherlands)

3. Results and Discussion

3.1. Vacancy Formation Energy and the Diffusion Path of Fe^{2+} Ions

As shown in Table 4, the vacancy formation energy of Fe^{2+} ions at octahedral site was 3.859 eV/atom, which was lower than that of Fe^{3+} ions at tetrahedral site in Fe_3O_4 crystal lattice. However, the vacancy formation energy of Fe^{2+} ions at octahedral site was 6.518 eV/atom, which was higher than that of Fe^{2+} ions at tetrahedral site in $FeAl_2O_4$. In addition the he vacancy formation energy of Fe^{2+} ions at tetrahedral site was 3.542 eV/atom and it was obviously lower than that of Cr^{3+} ions at octahedral site. According to the data in Table 4, Fe^{2+} ions tended to diffuse through the vacancy at tetrahedral site in Cr_2FeO_4 and $FeAl_2O_4$, but diffuse through the octahedral vacancy in Fe_3O_4. The calculated result was in agreement with the research of Freer [29].

Table 4. Vacancy formation energy in the octahedral and tetrahedral site in the lattice of Fe_3O_4, Cr_2FeO_4, and $FeAl_2O_4$ (eV/atom).

Lattice	Fe_3O_4	$FeAl_2O_4$	Cr_2FeO_4
Tetrahedral site	5.781(Fe^{3+})	4.259(Fe^{2+})	3.542(Fe^{2+})
Octahedral site	3.859(Fe^{2+})	6.518(Fe^{2+})	7.928(Cr^{3+})

3.2. Energy Barrier of the Diffusion of Fe^{2+} Ions

According to the diffusion path discussion in Section 3.1, the energy barrier of Fe^{2+} ions diffusion in Fe_3O_4, $FeAl_2O_4$, and Cr_2FeO_4 were calculated by molecular dynamics method. As shown in Figure 2, the energy barrier of the Fe^{2+} ions diffusion in Cr_2FeO_4 was higher than that in $FeAl_2O_4$, and obviously higher than that in Fe_3O_4 at 0 K. The result in Figure 2 indicated that the Fe^{2+} ions were prone to diffuse in Fe_3O_4, which also meant that the $FeAl_2O_4$ and Cr_2FeO_4 could effectively inhibited the diffusion of Fe^{2+} ions.

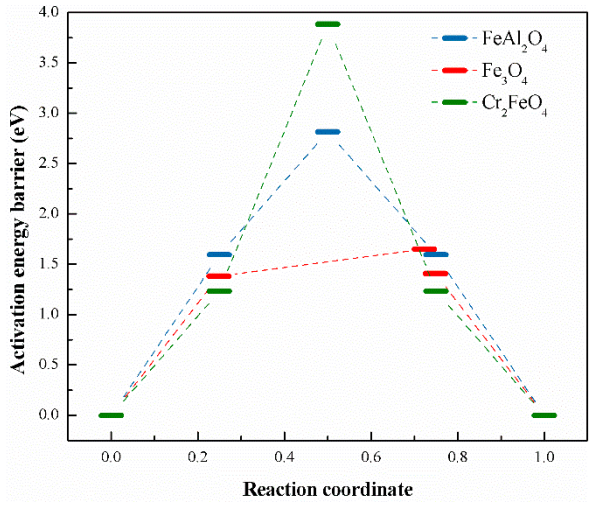

Figure 2. Energy barriers for an Fe^{2+} ion diffusing between octahedral sites in Fe_3O_4 and $FeAl_2O_4$ crystals respectively, calculated by the nudged elastic band (NEB) method at 0 K.

According to the result in Figure 3, when temperature ranged from 1073 to 1523 K, the energy barrier of Fe^{2+} ions diffusion in Cr_2FeO_4 was higher than that of $FeAl_2O_4$, and both of them were still obvious higher than that in Fe_3O_4. The variation rule of the diffusion energy barrier with temperature was shown in Figure 4, which was obtained by a summarization of data in Figure 3. As shown in Figure 4, the energy barrier of Fe^{2+} ions diffusion decreased with the increasing of temperature, but the energy barrier of Fe^{2+} ions diffusion in Cr_2FeO_4 and $FeAl_2O_4$ were still obviously higher than that in Fe_3O_4, which indicated an excellent inhibition effect of Cr_2FeO_4 and $FeAl_2O_4$ on diffusion of Fe^{2+} ions diffusion at the temperature ranging from 1073 to 1325 K. Compared with Cr_2FeO_4, $FeAl_2O_4$ could be prepared from a wide range of raw materials. Therefore, $FeAl_2O_4$ was selected as the interface layer to prepare a new anti-oxidation coating to protect the carbon steel S235JR at 1200 °C for 2 h.

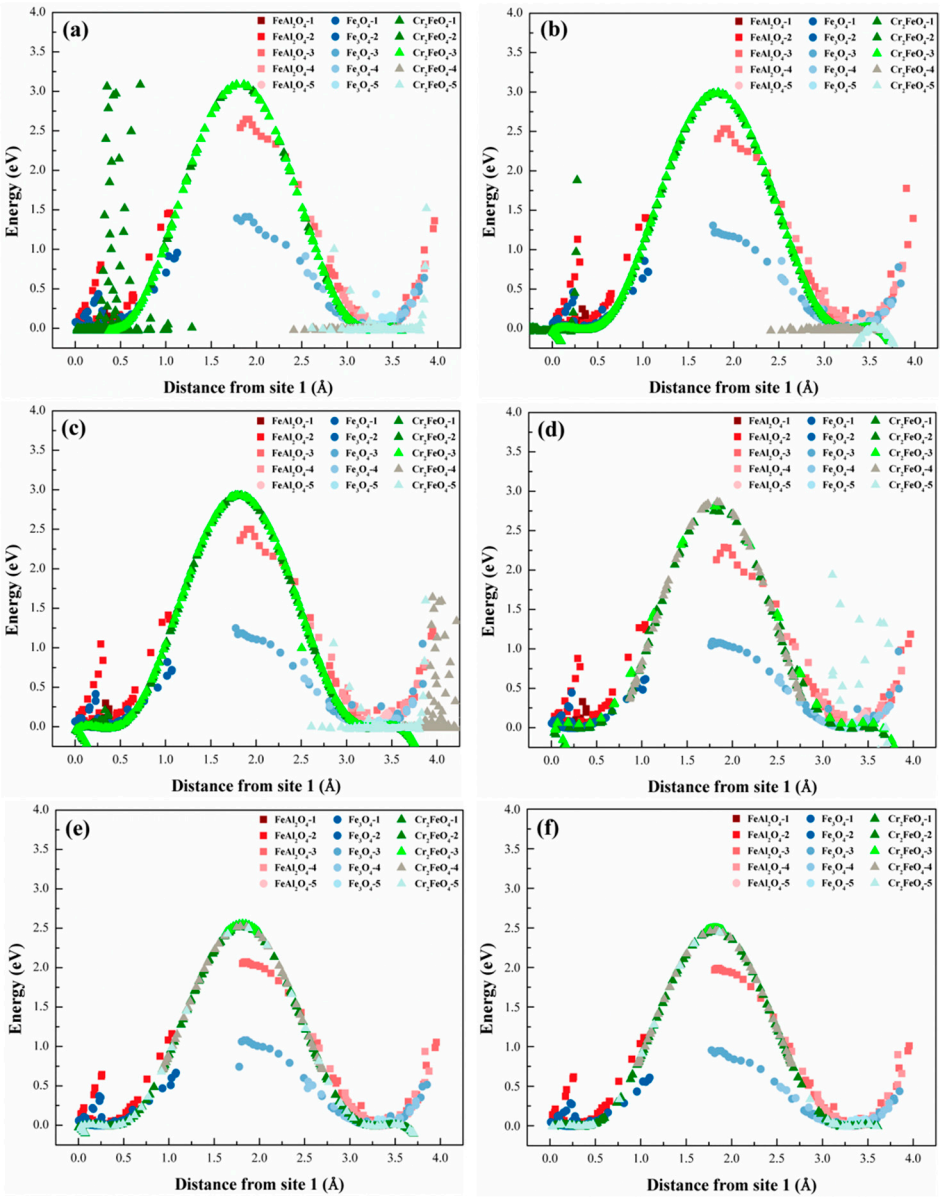

Figure 3. Energy barrier of Fe^{2+} ion diffusion in the crystal of Fe_3O_4, $FeAl_2O_4$, and Cr_2FeO_4 at different temperature: (**a**) 800 °C, (**b**) 900 °C, (**c**) 1000 °C, (**d**) 1100 °C, (**e**) 1200 °C, (**f**) 1250 °C.

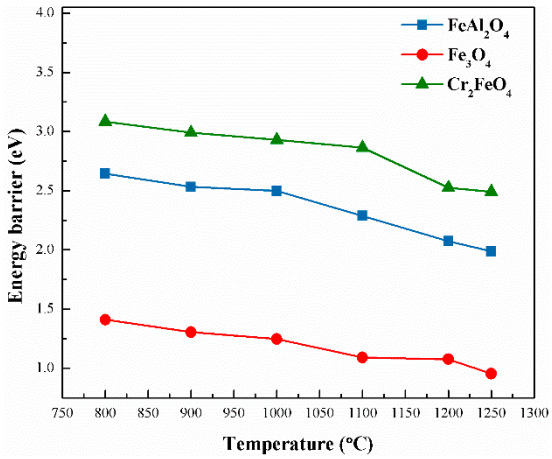

Figure 4. The comparison of the energy barrier of Fe^{2+} ion in the crystal of Fe_3O_4, $FeAl_2O_4$, and Cr_2FeO_4 at different temperature.

3.3. Anti-Oxidation Effect of the Coating

As shown in Figure 5a, the oxidation weight gain per unit area of coated sample during the temperature-rising process as well as the temperature-holding stage were obviously lower than those of bare sample, indicating that the prepared coating exhibited excellent anti-oxidation effect for S235JR.

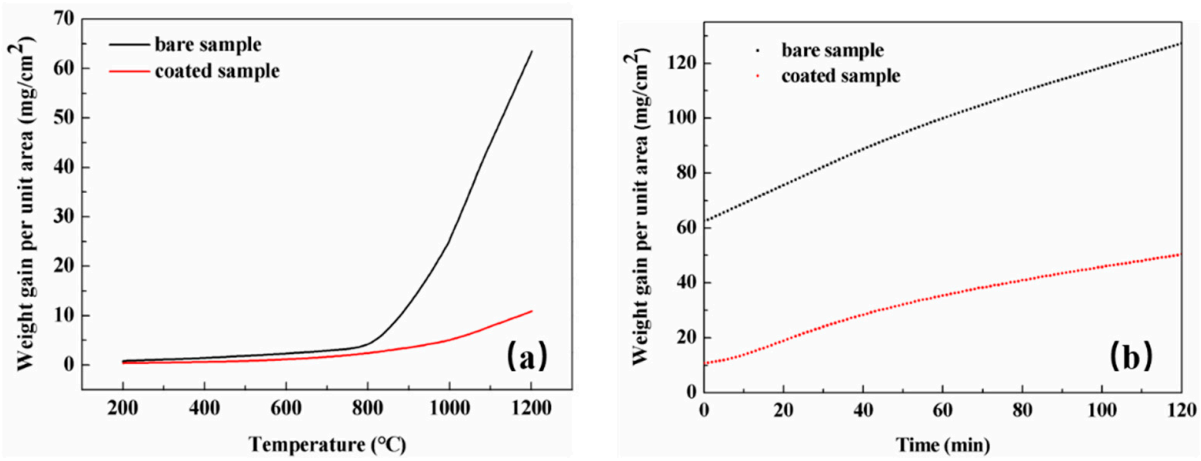

Figure 5. The curve of weight gain per unit area during the temperature-rising process of S235JR bare sample and coated sample at different stage (**a**) temperature-rising stage (**b**) temperature-holding stage.

According to the correlation coefficients shown in the Figure 6a, the oxidation kinetics of the bare sample agreed better with the linear law from 0 to 65 min, namely, the oxidation rate at this stage was controlled by the oxidation reaction, which mainly effected by the partial pressure of oxygen. While oxidation kinetics of the bare sample was described well with the parabolic law from 65 to 120 min, which meant that the oxidation rate at this stage controlled by ions diffusion. The weight gain of the coated sample was refitted with the same method, and the result was shown in Figure 6b. The oxidation kinetics of the coated sample was fitted well with the linear law from 0 to 10 min, while that of coated sample was well described by the parabolic law from 10 to 120 min.

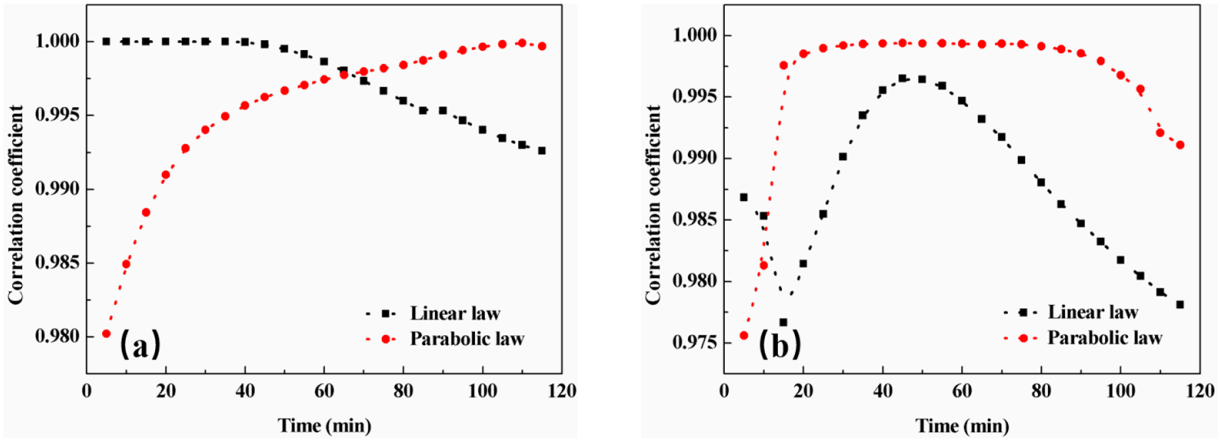

Figure 6. The comparison of the correlation coefficient of linear law and parabolic law (**a**) bare sample (**b**) coated sample.

Both the reaction rate constant at different stage of the coated sample and bare sample were calculated with the slope in Figure 7. The result in Figure 7 indicated that the coating exhibited excellent protective effect not only at the oxidation reaction-controlled stage, but also at the ions diffusion-controlled stage. According to the oxidation characterization at different stage, it was deduced that the prepared coating could effectively isolate the substrate from oxygen due to a lower oxidation rate constant at the stage following linear law, and that the coating could effectively inhibit the ions diffusion at high temperature due to a lower oxidation rate constant at the stage following parabolic law.

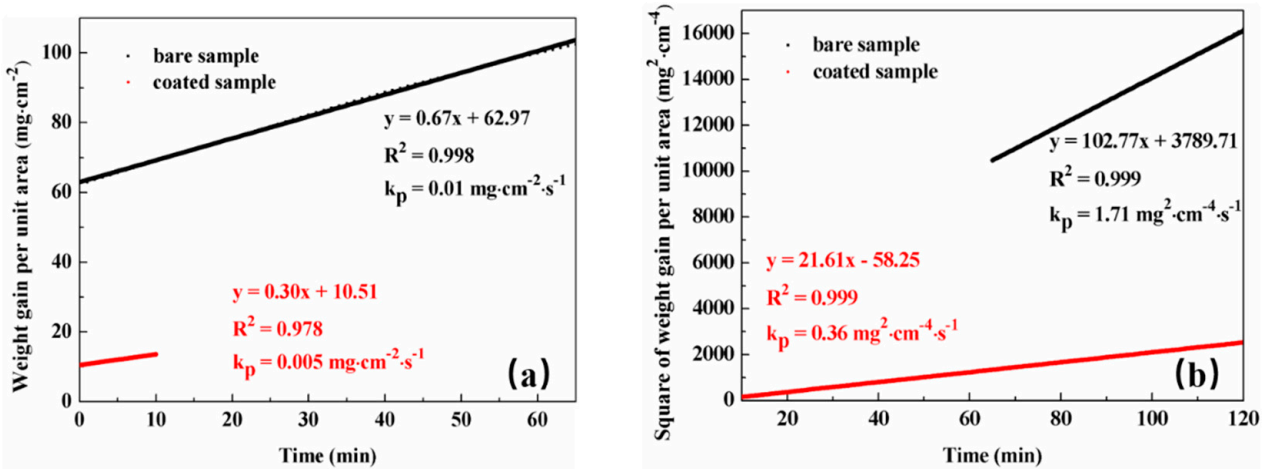

Figure 7. Result of isothermal oxidation kinetics of the bare sample and coated sample at different stage (**a**) the kinetics followed linear law (**b**) the kinetics followed parabolic law.

As shown in Figure 8, when heated at 1200 °C for 2 h, the diffusion distance of Fe element in the oxide layer of the coated sample continued to increase with the extension of holding time. However, it was always lower than that of the bare sample, further indicating that the prepared ceramic coating effectively inhibited the diffusion of Fe^{2+} ions.

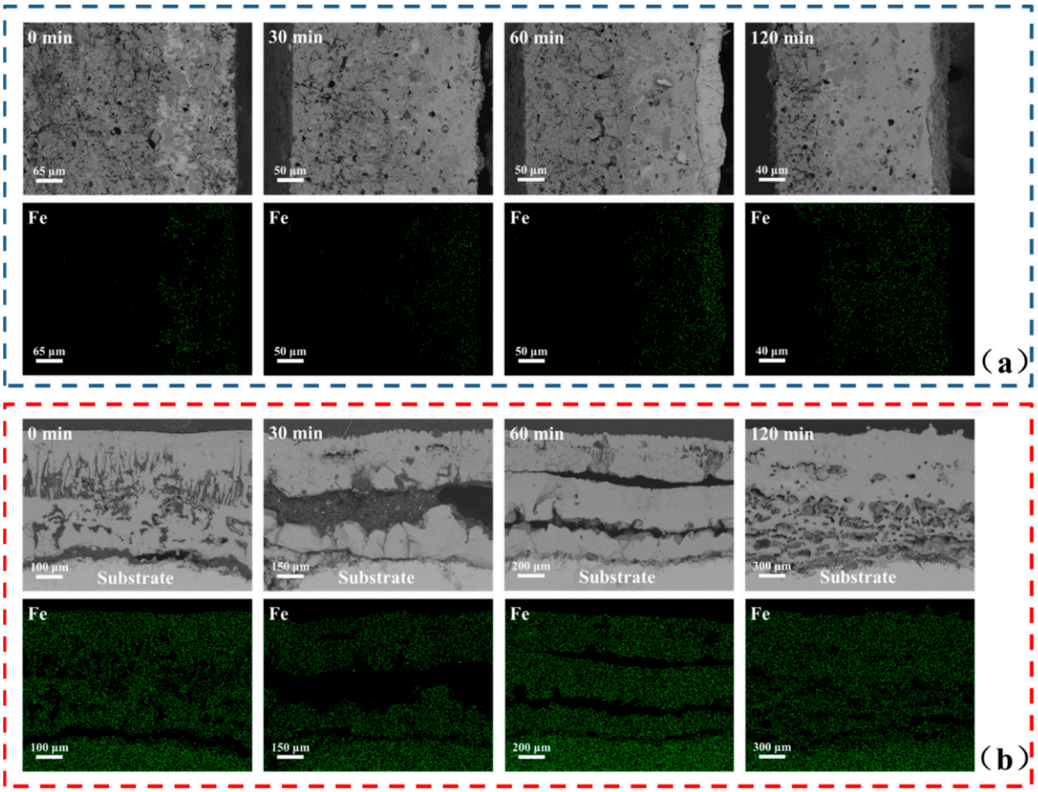

Figure 8. Fe element distribution within the oxide scale of S235JR bare sample and coated sample at 1200 °C for 2 h (**a**) coated sample (**b**) bare sample.

According to the X-ray energy spectrum of oxide layer (Figure 9), the prepared coating consisted of two layers. The outer layer was made of element Si and Al oxide, which could be deduced as sintering layer of mullite due to the atom ratio of energy dispersive spectrometer (EDS) result. Comparing with the kinetics result at the stage following linear law, the sintering layer contribute to form a compact structure, which could isolate the substrate from oxygen. The inner layer consisted of Fe and Al oxide, of which the atom ratio was similar to $FeAl_2O_4$. As shown in Figure 10, there was obviously phase peak of $FeAl_2O_4$ rather than the Fe oxide. In addition, the phase peak of the solid solution of Fe_2O_3-Al_2O_3 was similar to that of $FeAl_2O_4$, but the phase peak of the solid solution of Fe_2O_3-Al_2O_3 was offset to the small angle position due to the lattice distortion. According to the difference between the phase peak of $FeAl_2O_4$ and the solid solution of Fe_2O_3-Al_2O_3, the formation of interface of $FeAl_2O_4$ could be distinguished from the Fe oxide and the solid solution of Fe_2O_3-Al_2O_3 based on the X-ray diffraction (XRD) result in Figure 10. In addition, the peak of the amorphous phase at the small angle from 10 to 20 °could be explained by the liquid phase containing Si oxide. Combined with the XRD result in Figure 10 and EDS result in Figure 9, the formation of $FeAl_2O_4$ interface layer could be proved. Therefore, the forming structure comply with the design principle of coating, and the anti-oxidation coating with $FeAl_2O_4$ served as interface layer could effectively prevent the oxidation loss of carbon steel at high temperature.

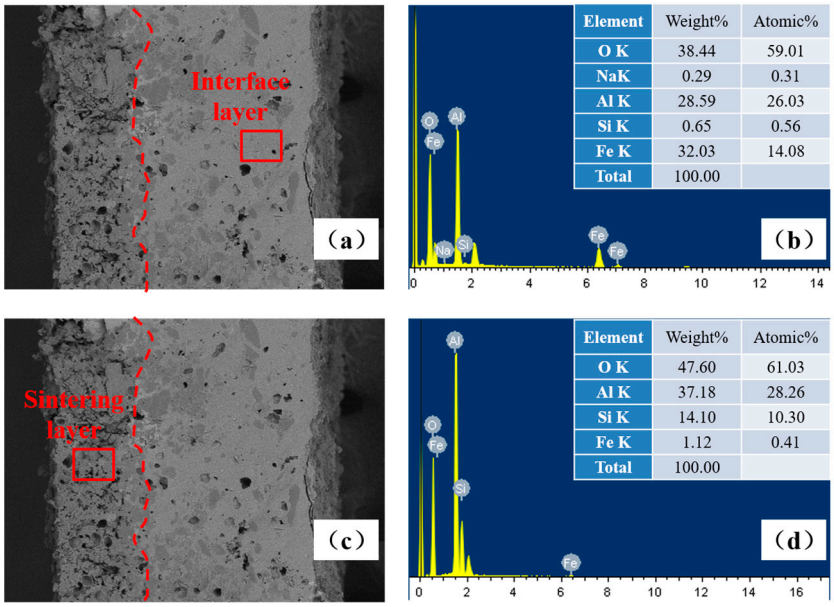

Figure 9. Energy dispersive spectrometer (EDS) point-scanning results of the oxide scale of S235JR coated sample protected by ceramic coating based on mullite (**a**) scanning area diagram of the interface layer (**b**) energy dispersive spectrometer result of the interface layer (**c**) scanning area diagram of the sintering layer (**d**) energy dispersive spectrometer result of the sintering layer.

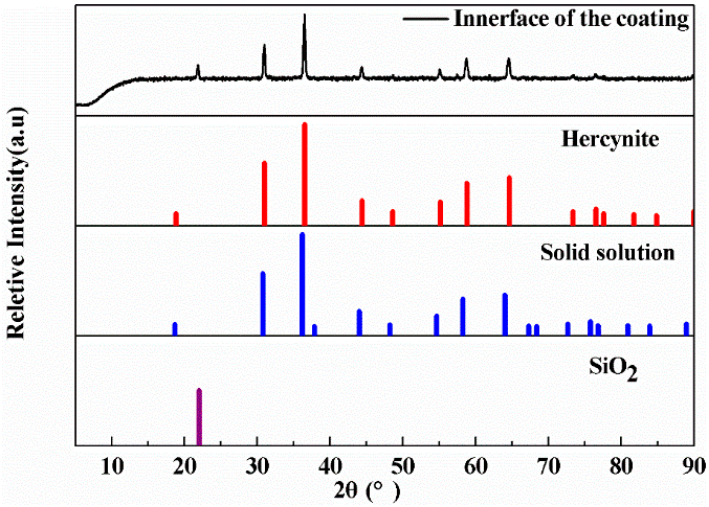

Figure 10. X-ray diffraction (XRD) result of the coating inner-face at 1200 °C for 120 min

As shown in Figure 11, residual oxide scale at the surface of the substrate was mainly consisted of element Fe and O, while Si and Al hardly occurred in the residual oxide scale, namely, the prepared coating were not harmful to the surface quality of the substrate. In addition, the gap between the coating and the substrate indicated that the coating could descaled from the substrate due to the difference of the thermal expansion coefficient during the cooling process.

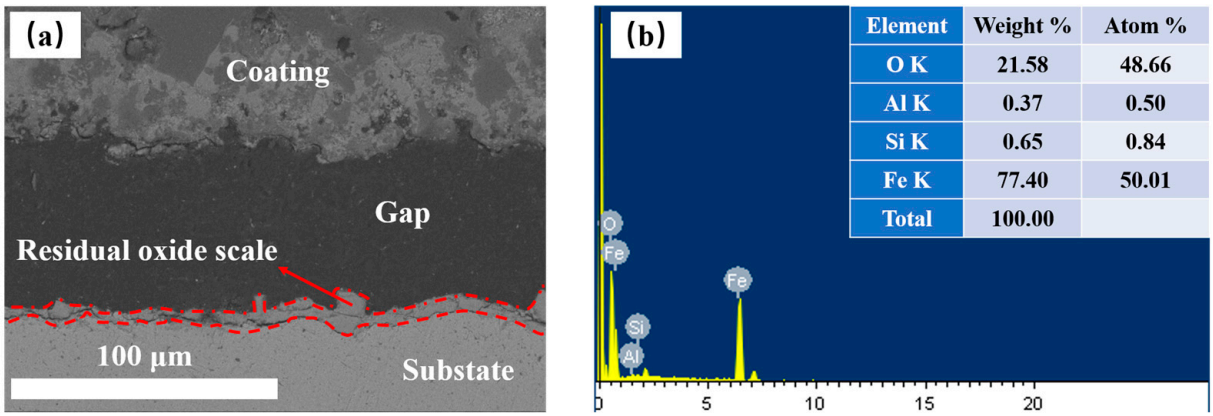

Figure 11. Energy dispersive spectrometer (EDS) result of the residual oxide scale of the coated sample at 1200 °C for 120 min (**a**) scanning area diagram of the residual oxide scale (**b**) energy dispersive spectrometer result of the residual oxide scale.

4. Conclusions

Referring to the theory of metal oxidation at high temperature, a mechanism of anti-oxidation coating design based on the inhibition effect of the interface layer on the diffusion of ions within oxide scale was introduced in this paper. According to the mechanism, a new ceramic coating was prepared to protect the carbons steel S235JR at 1200 °C for 2h. The mechanism was verified with the anti-oxidation effect of the coating and structure of the interface layer.

Some results were obtained as follows:

(1) The vacancy formation energy of Fe^{2+} in Fe_3O_4, $FeAl_2O_4$, and Cr_2FeO_4 was calculated by molecular dynamics method of Nudged elastic bond. The diffusion path of Fe^{2+} ions were analyzed by comparing the cationic defect formation energy at tetrahedral and octahedral sites in the crystal lattice above. The result indicated that Fe^{2+} ions tended to diffuse through the vacancy at tetrahedral site in Cr_2FeO_4 and $FeAl_2O_4$, but diffuse through the octahedral vacancy in Fe_3O_4.

(2) The Fe^{2+} ions diffusion energy barrier under the corresponding path conditions were calculated to verify the inhibition effect of Cr_2FeO_4 and $FeAl_2O_4$ on Fe^{2+} ions diffusion at high temperature. It could be indicated that when temperature ranged from 1073 to 1325 K, the energy barrier of Fe^{2+} ions diffusion in Cr_2FeO_4 was higher than that of $FeAl_2O_4$, and both of that were still obvious higher than that in Fe_3O_4.

(3) A new anti-oxidation coating was prepared based on the inhibition of interface layer consisted of $FeAl_2O_4$ to protect the carbon steel S235JR at 1200 °C for 2 h. According to the curve of weight gain per unit area during the temperature-rising process and temperature-holding stage, the oxidation loss of the substrate obviously decreased with the help of the coating. In addition, the oxidation rate constant of coated sample at the stage when the oxidation rate controlled by oxidation reaction was 0.005 $mg \cdot cm^{-2} \cdot s^{-1}$, which was much lower than that of bare sample (0.01 $mg \cdot cm^{-2} \cdot s^{-1}$). It suggested that the prepared coating could effectively isolate the substrate from oxygen. The oxidation rate constant of coated sample at the stage when the oxidation rate controlled by ions diffusion was 0.36 $mg^2 \cdot cm^{-4} \cdot s^{-1}$, which was much lower than that of bare sample (1.71 $mg^2 \cdot cm^{-4} \cdot s^{-1}$), indicating that the coating could effectively inhibit the ions diffusion at high temperature.

(4) The design principle of the coating based on the inhibition effect of interface layer on the diffusion of Fe^{2+} ions was verified by the X-ray energy spectrum of cross-section of the coating and the XRD result of coating inner face. The $FeAl_2O_4$ region was formed and observed at the interface between coating and Fe element diffusion area, and the mullite phase was distributed outside of the $FeAl_2O_4$ region.

Author Contributions: Conceptualization, B.Y., L.W., and S.Y.; Formal analysis, B.Y., Y.L., and L.W.; Funding acquisition, S.Y.; Investigation, B.Y., Y.D., and Y.W.; Methodology, B.Y. and L.W.; Software, B.Y. and Y.L.; Supervision, X.Z and S.Y.; Writing—original draft, B.Y.; Writing—review and editing, B.Y., Y.L., X.Z., and S.Y. All authors have read and agreed to the published version of the manuscript.

Funding: This research was funded by the Chinese academy of science project (No. KFJ-STS-QYZD-044) and National Key R&D Program during the 13th Five-year Plan Period (2019YFC1908405) to support this work.

Conflicts of Interest: The authors declare no conflict of interest.

References

1. Zhou, X.; Ye, S.F.; Xu, H.W.; Liu, P.; Wang, X.J.; Wei, L.Q. Influence of ceramic coating of MgO on oxidation behavior and descaling ability of low alloy steel. *Surf. Coat. Technol.* **2012**, *206*, 3619–3625. [CrossRef]
2. Wang, X.; Zhu, S.L.; Li, Z.X.; Chang, L.T.; Wu, Q.; Zhang, Y.S.; Wang, F.H. Oxidation behavior of a glass-based composite coating with a low expansion cermet bond-coat and an AlN diffusion barrier on K417G superalloy. *Corros. Sci.* **2018**, *145*, 283–294. [CrossRef]
3. Yu, B.; Fu, G.Y.; Cui, Y.B.; Zhang, X.M.; Tu, Y.B.; Du, Y.C.; Zuo, G.H.; Ye, S.F.; Wei, L.Q. Influence of Silicon-Modified Al Powders (SiO2@Al) on Anti-oxidation Performance of Al_2O_3-SiO_2 Ceramic Coating for Carbon Steel at High Temperature. *Coatings* **2019**, *9*, 167. [CrossRef]
4. Fu, G.Y.; Wei, L.Q.; Zhang, X.M.; Cui, Y.B.; Lv, C.C.; Ding, J.; Yu, B.; Ye, S.F. A high-silicon anti-oxidation coating for carbon steel at high temperature. *Surf. Coat. Technol.* **2017**, *310*, 166–172. [CrossRef]
5. Liu, P.; Wei, L.Q.; Zhou, X.; Ye, S.F. A glass-based protective coating on stainless steel for slab reheating application. *J. Coat. Technol. Res.* **2011**, *8*, 149–152. [CrossRef]
6. Chen, R.Y.; Yeun, W.Y.D. Review of the High-Temperature Oxidation of Iron and Carbon Steels in Air or Oxygen. *Oxid. Met.* **2003**, *59*, 433–468. [CrossRef]
7. Liu, P.; Wei, L.Q.; Ye, S.F.; Xu, H.W.; Chen, Y.F. Protecting stainless steel by glass coating during slab reheating. *Surf. Coat. Technol.* **2011**, *205*, 3582–3587. [CrossRef]
8. Abuluwefa, H.; Guthrie, R.I.L.; Ajersch, F. The effect of oxygen concentration on the oxidation of low-carbon steel in the temperature range 1000 to 1250 °C. *Oxid. Met.* **1996**, *46*, 423–440. [CrossRef]
9. Young, D.J.; Smeltzer, W.W.; Kirkaldy, J.S. The effects of molybdenum additions to nickel-chromium alloys on their sulfidation properties. *Metall. Mater. Trans. A* **1975**, *6*, 1205–1215. [CrossRef]
10. Sheasby, J.S.; Boggs, W.E.; Turkdogan, E.T. Scale growth on steels at 1200 °C: Rationale of rate and morphology. *Met. Sci.* **1984**, *18*, 127–136. [CrossRef]
11. Gleeson, B.; Hadavi, S.M.M.; Young, D.J. Isothermal transformation behavior of thermally-grown wüstite. *Mater. High. Temp.* **2000**, *17*, 311–318. [CrossRef]
12. Chen, R.Y.; Yuen, W.Y.D. The effects of steel composition on the oxidation kinetics, scale structure, and scale-steel interface adherence of low and ultra-low carbon steels. *Mater. Sci. Forum* **2006**, *522–523*, 451–460. [CrossRef]
13. Matsund, F. Blistering and hydraulic removal of scale films of rimmed steel at high-temperature. *Trans. Iron Steel Inst. Jpn.* **1980**, *20*, 413–421. [CrossRef]
14. Dieckmann, R.; Schmalzried, H. Defects and Cation Diffusion in Magnetite (I). Ber. Bunsenges. *Physic. Chem.* **1977**, *81*, 344–347.
15. Frölich, F.; Stiller, H. The nature of chemical bond of magnetite and consequences. *Geofisica Pura E Appl.* **1963**, *55*, 91–100. [CrossRef]
16. Fu, G.Y.; Wei, L.Q.; Shan, X.; Zhang, X.M.; Ding, J.; Lv, C.C.; Liu, Y.; Ye, S.F. Influence of a Cr_2O_3 glass coating on enhancing the oxidation resistance of 20MnSiNb structural steel. *Surf. Coat. Technol.* **2016**, *294*, 8–14. [CrossRef]
17. Jastrzębska, I.; Szczerba, J.; Stoch, P.; Błachowski, A.; Ruebenbauer, K.; Prorok, R.; Śnieżek, E. Crystal structure and Mössbauer study of $FeAl_2O_4$. *Nukleonika* **2015**, *60*, 45–47. [CrossRef]
18. Odashima, H.; Kitayama, M. Oxidation inhibition mechanism and performance of a new protective coating for slab reheating of 3% Si-steel. *ISIJ. Int.* **1990**, *30*, 255–264. [CrossRef]
19. Henkelman, G.; Jónsson, H. Improved tangent estimate in the nudged elastic band method for finding minimum energy paths and saddle points. *J. Chem. Phys.* **2000**, *113*, 9978–9985. [CrossRef]
20. Zhou, X.W.; Wadley, H.N.G.; Filhol, J.S.; Neurock, M.N. Modified charge transfer-embedded atom method potential for metal/metal oxide systems. *Phys. Rev. B* **2004**, *69*, 035402. [CrossRef]
21. Zhou, X.W.; Wadley, H.N.G. A charge transfer ionic–embedded atom method potential for the O–Al–Ni–Co–Fe system. *J. Phys. Condens. Matter* **2005**, *17*, 3619–3635. [CrossRef]
22. Plimpton, S. Fast parallel algorithms for short-range molecular dynamics. *J. Comput. Phys.* **1995**, *117*, 1–19. [CrossRef]
23. Stukowski, A. Visualization and analysis of atomistic simulation data with OVITO-the Open Visualization Tool. *Model. Simul. Mater. Sci. Eng.* **2010**, *18*, 015012. [CrossRef]
24. Jastrzebska, I.; Szczera, J.; Blachowski, A.; Stoch, P. Structure and microstructure evolution of hercynite spinel ($Fe^{2+}Al_2O_4$) after annealing treatment. *Eur. J. Mineral.* **2017**, *28*, 1–11.

25. Rodríiguez, E.; Castillo, G.; Contreras, J.; Puente-Ornelas, R.; Aguilar-Martínez, J.A.; García, L.; Gómez, C. Hercynite and magnesium aluminate spinels acting as a ceramic bonding in an electrofused MgO-$CaZrO_3$ refractory brick for the cement industry. *Ceram. Int.* **2012**, *38*, 6769–6775. [CrossRef]
26. Dong, Y.C.; Lu, H.; Cui, J.; Yan, D.R.; Yin, F.X.; Li, D.Y. Mechanical characteristics of $FeAl_2O_4$ and $AlFe_2O_4$ spinel phases in coatings-A study combining experimental evaluation and first-principles calculations. *Ceram. Int.* **2017**, *43*, 16094–16100. [CrossRef]
27. Stempkowska, A.; Mastalska-Poplawska, J.; Izak, P. Stabilization of kaolin clay slurry with sodium silicate of different silicate moduli. *Appl. Clay. Sci.* **2017**, *146*, 147–151. [CrossRef]
28. Boisvert, J.P.; Persello, J.; Castaing, J.C.; Cabane, B. Dispersion of aluminum-coated TiO_2 particles by absorption of sodium polyacrylate. *Colloid. Surf.* **2001**, *178*, 187–198. [CrossRef]
29. Freer, R.; Oreilly, W. The diffusion of Fe^{2+} ions in spinels with relevance to the process of maghemitization. *Miner. Mag.* **1980**, *43*, 889–899. [CrossRef]